J|A|C|S ARTICLES

Published on Web 08/28/2009

Mesomorphic Imidazolium Salts: New Vectors for Efficient siRNA Transfection

William Dobbs,[†] Benoît Heinrich,[†] Cyril Bourgogne,[†] Bertrand Donnio,[†] Emmanuel Terazzi,[†] Marie-Elise Bonnet,[‡] Fabrice Stock,[‡] Patrick Erbacher,[‡] Anne-Laure Bolcato-Bellemin,[‡] and Laurent Douce*,[†]

Institut de Physique et Chimie des Matériaux de Strasbourg, UMR 7504, CNRS-Université de Strasbourg, BP 43, 23 rue du Loess, F-67034 Strasbourg Cedex 2, France, and Polyplus-transfection, BIOPARC, Boulevard Sébastien Brandt, BP 90018, 67401 Illkrich, France

Received April 21, 2009; E-mail: Laurent.Douce@ipcms.u-strasbg.fr

Abstract: The preparation of chloride (**1**$_n$) and bromide (**2**$_n$) derivatives of 1-methyl-3-[3,4-bis(alkoxy)benzyl]-4*H*-imidazolium with $n = 6$, 12, 16, 18 is described. The two series of salts possess a rich thermotropic mesomorphism, chain-length dependent. Thus, a lamellar smectic A phase, a bicontinuous cubic $Ia\bar{3}d$ phase, and a columnar hexagonal liquid crystalline mesophase are induced as a function of increasing chain length. The mesomorphic properties were studied by polarizing optical microscopy, differential scanning calorimetry, and X-ray diffraction, and with the support of dilatometry and molecular dynamics, models for the various supramolecular arrangements of the salts are proposed. Such cationic amphiphiles were expected to be candidate molecules to design a new delivery reagent for nucleic acid transfection, particularly for short interfering RNA (siRNA). The use of an RNA interference mechanism, by introduction into cells by transfection of chemically synthesized siRNAs, is a powerful method for gene silencing studies. To exploite the potential of these amphilic imidazolium salts, these molecules were formulated with cohelper lipids and tested for their efficacy to deliver active siRNAs. Our results show high transfection efficacy of our formulated compounds and high silencing efficiency with more than 80% inhibition of the targeted gene at 10 nM siRNA concentration. Taken together our results show the potency of amphiphilic imidazolium salts as a new generation of transfection reagents for RNA interference.

1. Introduction

Uniting the properties of ionic derivatives—their low melting points, low volatility, nonflammability, high chemical and radiochemical stability, tunable conductivity, and wide electrochemical windows—with those of liquid crystals, with their many forms of labile macroscopic ordering, raises fascinating prospects. This combination could lead to a vast range of new multifunctional materials.[1] Ionic molecules have also attracted much attention in the fields of biorelated sciences, a major reason for this interest being the ability of appropriate cationic compounds to form liposomes able to confine anionic species, DNA being one example, by Coulombic interactions.[2] The description of cationic amphiphiles active as nucleic acid transfection agents,[3] in particular, has sparked major interest within the scientific community.[4] An important application of this procedure, defined recently by A. Z. Fire and C. C. Mello,[5] concerns the fact that double-stranded RNA triggers suppression of gene activity in a homology-dependent manner, the RNA interference (RNAi) process. The ability of RNAi to dramatically and selectively reduce the expression of an individual protein in a cell makes RNAi a valuable laboratory tool, both in cell culture and *in vivo*. Furthermore, RNAi protects against RNA virus infections, especially in plants and invertebrate animals,

[†] CNRS-Université de Strasbourg.

[‡] Polyplus-transfection.

(1) (a) Wasserscheid, P.; Welton, T. *Ionic Liquids in Synthesis*; Wiley-VCH: Weinheim, 2003. (b) Dupont, J.; de Souza, R. F.; Suarez, P. A. *Chem. Rev.* **2002**, *102*, 3667–3692. (c) Song, C. E. *Chem. Commun.* **2004**, 1033–1043. (d) Ohno, H. *Electrochemical Aspects of Ionic Liquids*; Wiley-Interscience: 2005. (e) Crosthwaite, J. M.; Aki, S. N. V. K.; Maginn, E. J.; Brennecke, J. F. *J. Phys. Chem. B* **2004**, *108*, 5113–5119. (f) Yoshizawa, M.; Xu, W.; Angell, C. A. *J. Am. Chem. Soc.* **2003**, *125*, 15411–15419. (g) Fry, A. J. *J. Electroanal. Chem.* **2003**, *546*, 35–39. (h) *Ionic Liquids IIIA: Fundamental, Progress, Challenges and Opportunities*; Rogers, R. B., Seddon, K. R., Eds.; ACS Symposium Series 901; American Chemical Society: Washington DC, 2005. (i) *Ionic Liquids IIIB: Fundamental, Progress, Challenges and Opportunities*; Rogers, R. B., Seddon, K. R., Eds.; ACS Symposium Series 902; American Chemical Society: Washington DC, 2005.

(2) (a) Rädler, J. O.; Koltover, I.; Salditt, T.; Safinya, C. R. *Science* **1997**, *275*, 810–814. (b) Cui, L.; Zhu, L. *Lamgnuir* **2006**, 5982–5985. (c) Miller, A. D. *Angew. Chem., Int. Ed.* **1998**, *37*, 1768–1785. (d) Cui, L.; Miao, J.; Zhu, L. *Macromolecules* **2006**, *39*, 2536–2545. (e) Joester, D.; Losson, M.; Pugin, R.; Heinzelmann, H.; Walter, E.; Merkle, H. P.; Diederich, F. *Angew. Chem., Int. Ed.* **2003**, *42*, 1486–1490.

(3) (a) Huang, Q.-D.; Chen, H.; Zhou, L.-H.; Huang, J.; Wu, J.; Yu, X.-Q. *Chem. Bio. Drug Des.* **2008**, *71*, 224–229. (b) Ito, A.; Miyazoe, R.; Mitoma, J.; Akao, T.; Osaki, T.; Kunitake, T. *Biochem. Int.* **1990**, *22*, 235–241. (c) van der Woude, I.; Wagenaar, A.; Meekel, A. A.; ter Beest, M. B.; Ruiters, M. H.; Engberts, J. B.; Hoekstra, D. *Proc. Natl. Acad. Sci. U.S.A.* **1997**, *94*, 1160–1165. (d) Zhang, S.; Zhao, B.; Jiang, H.; Wang, B.; Ma, B. *J. Controlled Release* **2007**, *123*, 1–10.

(4) (a) Aigner, A. *Curr. Opin. Mol. Ther.* **2007**, *9*, 345–352. (b) Li, W.; Szoka, F. C. *Pharm. Res.* **2007**, *24*, 438–49.

(5) (a) Fire, A. Z. *Angew. Chem., Int. Ed.* **2007**, *46, 37*, 6966–6984. (b) Mello, C. C. *Angew. Chem., Int. Ed.* **2007**, *46, 37*, 6985–6994.

10.1021/ja903028f CCC: $40.75

Scheme 1. Synthetic Procedure[a]

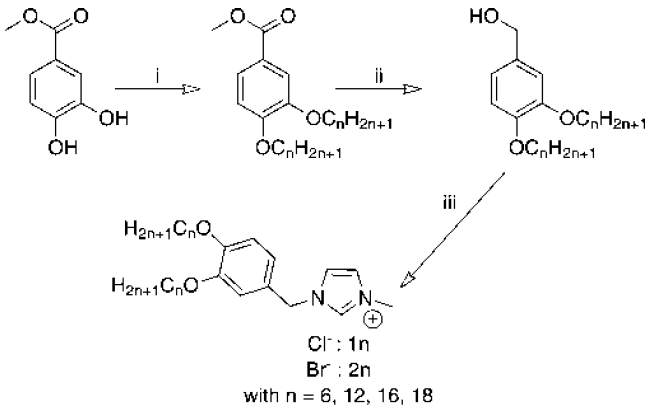

[a] (i) DMF, K_2CO_3, BrC_nH_{2n+1}, 70 °C; (ii) THF, $LiAlH_4$; (iii) CH_2Cl_2, $SOBr_2$, or $SOCl_2$ in THF or toluene, methylimidazole, N_2.

and ensures genome stability by keeping mobile elements silent. Despite the current interest in cationic compounds for RNAi delivery, it seems that only a few examples using an imidazolium salt backbone as a polar headgroup on a cationic lipid formulation have been investigated.[6] The present article concerns a synthetic route to amphiphilic imidazolium salts, which not only exhibit thermotropic liquid crystal behavior but also are capable of forming lipoplexes with nucleic acids. In association with a colipid (dioleoyl phosphatidylethanolamine, DOPE), these amphiphilic imidazolium salts are able to deliver siRNAs into cells, leading then to efficient and specific endogenous gene silencing. The ability of our amphiphilic imidazolium-based formulations to complex chemically synthesized siRNA was evaluated. Gene silencing efficiency of imidazolium/siRNA complexes was examined on a human lung carcinoma cell line stably expressing the luciferase (A549Luc) gene. Moreover the particle size and zeta potential of the complex were measured. Taken together our data showed the great potency of our imidazolium salts to deliver active siRNAs into cells and point out a new generation of efficient nonviral reagents for siRNA delivery.

2. Results and Discussion

2.1. Synthesis. Chloride ($\mathbf{1}_n$) and bromide ($\mathbf{2}_n$) derivatives of 1-(3,4-bis(alkyloxy)benzyl)-3-methyl-1*H*-imidazo-3-ium with n = 6, 12, 16, 18 have been synthesized in good yield, on the gram scale. These compounds were obtained in three steps, following slightly modified literature procedures.[7] Methyl 3,4-dihydroxybenzoate was etherified with various 1-bromoalkanes ($C_nH_{2n+1}Br$, n = 6, 12, 16, 18) in the presence of K_2CO_3 in DMF, and the resulting amphipathic esters reduced by $LiAlH_4$ into the corresponding benzyl alcohols. The different resulting alcohols were converted into 3,4-bis(alkoxy)benzyl chlorides or bromides with either thionyl chloride or thionyl bromide in quantitative yields. The final compounds $\mathbf{1}_n$ and $\mathbf{2}_n$ were obtained by quaternalization of 1-methylimidazole with the chlorides and bromides under refluxing toluene or THF in inert atmosphere (Scheme 1). The final compounds were purified by flash chromatography or crystallization and characterized by ^{1}H NMR, ^{13}C NMR{^{1}H}, FT-IR spectroscopy, and elemental analysis.

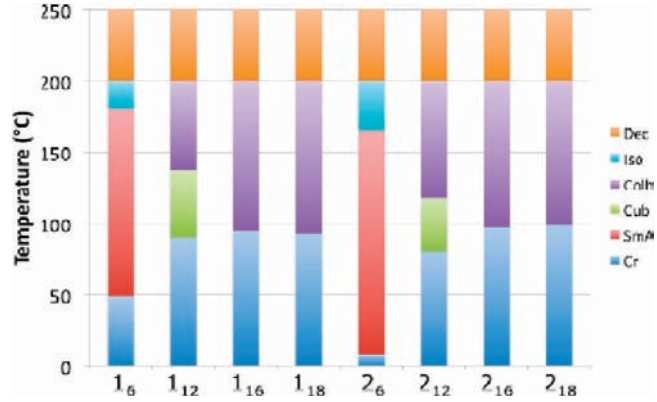

Figure 1. Phase and temperature transitions as a function of the alkyl chain length (Cr = Crystal, SmA = smectic A phase, Cub = cubic phase, Colh = columnar hexagonal phase, Dec = decomposition temperature). The transition temperatures are assigned from the onset temperatures during heating cycles.

Distinctive signals assigned to the CH group at the 2-position of the imidazolium ring appear in the ^{1}H NMR spectra of, for example, $\mathbf{1_{12}}$ and $\mathbf{2_{12}}$ at δ = 10.51 and 10.83 ppm and in the ^{13}C NMR{^{1}H} spectra at δ = 138.07 and 137.47 ppm, respectively. Synthesis of the siRNA was performed by Eurogentec (Seraing, Belgium) and is described in the Supporting Information.

2.2. Investigation of the Liquid Crystalline Behavior. As expected, all the ionic compounds $\mathbf{1}_n$ and $\mathbf{2}_n$ show liquid crystal properties.[8] The mesomorphic properties and the phase transition temperatures were preliminarily studied by differential scanning calorimetry (DSC) and polarizing microscopy (POM). These data are summarized in Figure 1.

The melting temperatures of all the compounds with $n > 6$ show a low dependence upon chain length and are quasi counteranion invariant (between 80−100 °C); the first homologues of the series are nearly ($\mathbf{1_6}$) or room-temperature liquid crystals ($\mathbf{2_6}$). Decomposition was however systematically detected for all the other compounds above 200 °C, that is in the isotropic liquid for $\mathbf{1_6}$ and $\mathbf{2_6}$ (clearing temperatures 180 and 165 °C, respectively, for the SmA-I phase transformation temperatures) and still in the mesophase for the other members of the series. The mesophases' nature could be quite easily assigned on the basis of their optical textures. Thus, a smectic A (SmA) lamellar arrangement was induced for the short alkyl chain-length homologues ($\mathbf{1_6}$ and $\mathbf{2_6}$): on cooling from the isotropic liquid, the samples appeared black (uniform homeotropic texture) when viewed under cross polarizers alongside alignment-induced birefringent defects near trapped air bubbles.

(6) (a) Mével, M.; Breuzard, G.; Yaouanc, J.-J.; Clément, J.-C.; Lehn, P.; Pichon, C.; Jaffrés, P.-A.; Midoux, P. *ChemBioChem* **2008**, *9*, 1462–1471. (b) Midoux, P.; Pichon, C.; Yaouanc, J.-J.; Jaffrés, P. *Br. J. Pharmacol.* **2009**, *157*, 166–178.

(7) Dobbs, W.; Douce, L.; Allouche, L.; Louati, A.; Malbocs, F.; Welter, R. *New J. Chem.* **2006**, *30*, 528–532.

(8) (a) Binnemans, K. *Chem. Rev.* **2005**, *105*, 4148–4204. (b) Kato, T.; Misoshita, N.; Kishimoto, K. *Angew. Chem., Int. Ed.* **2006**, *45*, 38–68. (c) Yoshio, M.; Mukai, T.; Ohno, H.; Kato, T. *J. Am. Chem. Soc.* **2004**, *126*, 994–995. (d) Bowlas, C. J.; Bruce, D. W.; Seddon, K. R. *Chem. Commun.* **1996**, 1625–1626. (e) Gordon, C. M.; Holbrey, J. D.; Kennedy, A. R.; Seddon, K. R. *J. Mater. Chem.* **1998**, *8*, 2627–2636. (f) Bradley, A. E.; Hardacre, C.; Holbrey, J. D.; Johnston, S.; McMath, S. E. J.; Nieuwenhuyzen, M. *Chem. Mater.* **2002**, *14*, 629–635. (g) De Roche, J.; Gordon, C. M.; Imrie, C. T.; Ingram, M. D.; Ingram, A. R.; Kennedy, A. R.; LoCelso, F.; Triolo, A. *Chem. Mater.* **2003**, *15*, 2003. (h) Lee, K.-M.; Lee, Y.-T.; Lin, J. B. *J. Mater. Chem.* **2003**, *13*, 1079–1084. (i) Chiou, J. Y. Z.; Chen, J. N.; Lei, J. S.; Lin, I. J. B. *J. Mater. Chem.* **2006**, *16*, 2972–2977. (j) Yazaki, S.; Kamikawa, Y.; Yoshio, M.; Hamasaki, A.; Mukai, T.; Ohno, H.; Kato, T. *Chem. Lett.* **2008**, *37,5*, 528–539.

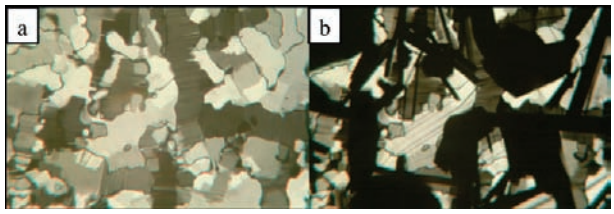

Figure 2. POM textures of $\mathbf{2_{12}}$ on cooling (a) in the columnar hexagonal phase at $T = 130$ °C and (b) at the transition to the cubic phase (formation of black polygonal areas).

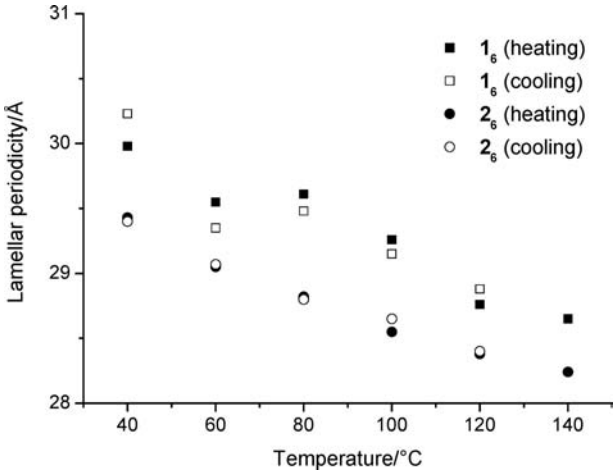

Figure 3. Temperature dependence of the lamellar SmA periodicities of $\mathbf{1_6}$ and $\mathbf{2_6}$.

For all the other homologues with a chain length greater than 12, a columnar phase was recognized by the observation of large, birefringent developing domains coalescing into a mosaic-like texture. For the intermediate compounds $\mathbf{1_{12}}$ and $\mathbf{2_{12}}$, on cooling (rapid first, and then slow) from 200 °C, the temperature at which decomposition starts to occur, the growth of a homogeneous mosaic-like texture was clearly observed (Figure 2a). On further cooling, the materials undergo a transition into a cubic phase, identified by the complete loss of birefringence and the formation of large black, optically extinct, highly viscous, polygonal areas (Figure 2b).

The identification of all the mesophases was supported by small-angle X-ray diffraction. SAXS patterns were collected for all the salts as a function of temperature. Typically, in all cases, a series of sharp and intense peaks were observed in the low-angle part of the diffractogram, characterizing the mesophase symmetry, while, in the large angle region, i.e., at *ca.* 4.5−4.6 Å, a very intense and diffuse scattering halo was observed, corresponding to the molten alkyl chain in liquid-like order.

Imidazolium salts $\mathbf{1_6}$ and $\mathbf{2_6}$ exhibit a layered structure over the whole mesomorphic temperature range, with two sharp and intense small-angle reflections, in the ratio 1:2, systematically observed on the diffractograms. In both systems (**1** and **2**), the smectic periodicity decreases with increasing temperature (see Tables 2 and 3 in Supporting Information), reflecting the higher thermal mobility of the alkyl chains, concomitant to the smectic layers' compression; this trend is perfectly reproducible, and the periodicity values can be quasi superimposed on both heating and cooling (Figure 3). Interestingly also, the periodicity of the chloride salts is always greater than that of the bromides, in concordance with the slightly larger ionic radius of the former ($r_{Cl^-} = 99.4$ pm $< r_{Br^-} = 114.5$ pm), and thus the larger cross-sectional area (vide infra).

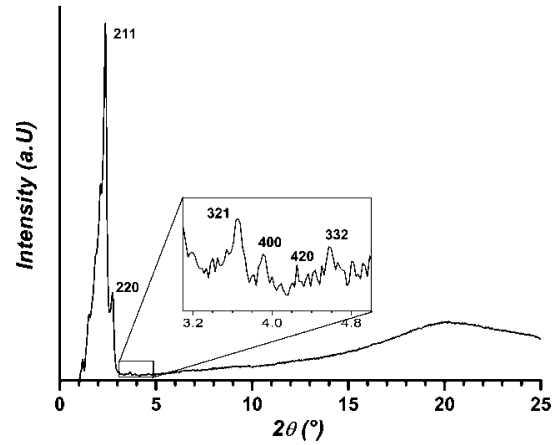

Figure 4. Diffraction small-angle X-ray pattern of the $Ia3\bar{d}$ cubic phase of $\mathbf{2_{12}}$ recorded at $T = 90$ °C.

The cubic symmetry for the intermediate mesophase of $\mathbf{1_{12}}$ and $\mathbf{2_{12}}$ was assigned unambiguously by SAXS measurements as belonging to the $Ia3\bar{d}$ space group. Up to six sharp reflections were detected in the low angle range for which the reciprocal *d*-spacings were in the ratios $\sqrt{3}$:$\sqrt{4}$:$\sqrt{7}$:$\sqrt{8}$:$\sqrt{10}$:$\sqrt{11}$. Since the ratio $\sqrt{7}$ is not compatible with a cubic symmetry [$(h^2+k^2+l^2)^{1/2} = a/d_{hkl}$)], the sequence of numbers must be doubled as $\sqrt{6}$:$\sqrt{8}$:$\sqrt{14}$:$\sqrt{16}$:$\sqrt{20}$:$\sqrt{22}$ (Figure 4, Table 1). Complete space group determination of mobile thermotropic cubic phases is difficult, although the large initial number of theoretical possibilities (36) can be reduced by logical analysis of the data, as shown below. In our standard diffraction experiment, all noncentrosymmetric groups (groups with Laue classes 23, 432, or 43*m*) can be disregarded on account of Friedel's law,[9] which leaves only 17 cubic space groups to consider. The sequence of the ratios is not compatible with a face-centered-cubic network (*F*) due to the presence of ratio $\sqrt{14}$ and is thus excluded. Similarly, primitive Bravais lattices (*P*) are highly improbable due to the unexplained absence of numerous authorized reflections. The reflections were therefore successfully indexed as (211), (220), (321), (400), (420), and (332) of a body-centered cubic network (*I*) with the cubic lattice parameter, *a*, in the 9 nm range for both $\mathbf{1_{12}}$ and $\mathbf{2_{12}}$ (Table 1). The extinction rule of the $Ia3\bar{d}$ space group[9] is theoretically compatible with this set of observed reflections; moreover, the strongest *hkl* reflections, (211) and (220), are the first reflections permitted by the $Ia3\bar{d}$ cubic space group.[10]

Finally, the XRD patterns recorded for the salts $\mathbf{1_{12}}$, $\mathbf{1_{16}}$, $\mathbf{1_{18}}$, $\mathbf{2_{12}}$, $\mathbf{2_{16}}$, and $\mathbf{2_{18}}$ are characterized by the presence of two up to four sharp small-angle X-ray reflections, depending on the sample, with reciprocal *d*-spacings in the ratio 1:$\sqrt{3}$:2:$\sqrt{7}$. These three features are most readily assigned as the (10), (11), (20), and (21) reflections of a columnar phase with a hexagonal lattice. The variation of the cross-columnar section area *S* ($S = {}^1/_2a^2\sqrt{3}$) was followed as a function of temperature for each of the derivatives (Figure 5 and Supporting Information). *S* is found

(9) [$0kl$:$k,l = 2n$, hhl:$2h + l = 4n$, $h00$:$h = 4n$, where *n* is an integer, and *h*, *k*, and *l* are permutable] *International Tables for Crystallography*, 4th ed.; Hahn, T., Ed.; The International Union of Crystallography; Kluwer Academic Publishers: Dordrecht, The Netherlands, Boston, London, 1995; Vol. A.

(10) (a) Diele, S. *Curr. Opin. Colloid Interface Sci.* **2002**, *7*, 333. (b) Kutsumizu, S. *Curr. Opin. Solid State Mater. Sci.* **2002**, *6*, 537. (c) Impéror-Clerc, M. *Curr. Opin. Colloid Interface Sci.* **2005**, *9*, 370. (d) Lynch, M. L.; Spicer, P. T. *Bicontinuous Liquid Crystals*; Taylor & Francis: 2005; p 127.

Table 1. Indexation of the Reflections Detected in the Cubic Liquid-Crystalline Phase by SAXS for Compounds $\mathbf{1_{12}}$ and $\mathbf{2_{12}}$ at a Given Temperature

		$\mathbf{1_{12}}$ at $T = 100$ °C			$\mathbf{2_{12}}$ at $T = 90$ °C		
hkl[a]	*I*/a.u.[b]	d_{meas}/Å[c]	d_{calcd}/Å[c]	parameters[d]	d_{meas}/Å[c]	d_{calcd}/Å[c]	parameters[d]
211	VS (sh)	37.12	37.16		37.03	37.00	
220	S (sh)	32.15	32.18	$a = 91.02$ Å	32.10	32.05	$a = 90.64$ Å
321	M (sh)	24.39	24.33	$V = 754068$ Å^3	24.38	24.22	$V = 744663$ Å^3
400	W (sh)	22.76	22.76	$N = 732$	22.46	22.66	$N = 730$
420	VW (sh)	20.36	20.35		20.28	20.26	
332	VW (sh)	19.38	19.41		19.31	19.32	

[a] Miller indices. [b] *I* corresponds to the intensity of the reflections (VS: very strong, S: strong; M: medium; W: weak; VW: very weak; br and sh stand for broad and sharp). [c] d_{meas} and d_{calcd} are the measured and calculated diffraction spacing. [d] Phase parameters: *a*, lattice parameter of the cubic phase; *V*, volume of the cubic cell (Å^3), and N, number of molecules within the cubic cell ($N = $ Å$^3/V_{mol}$).

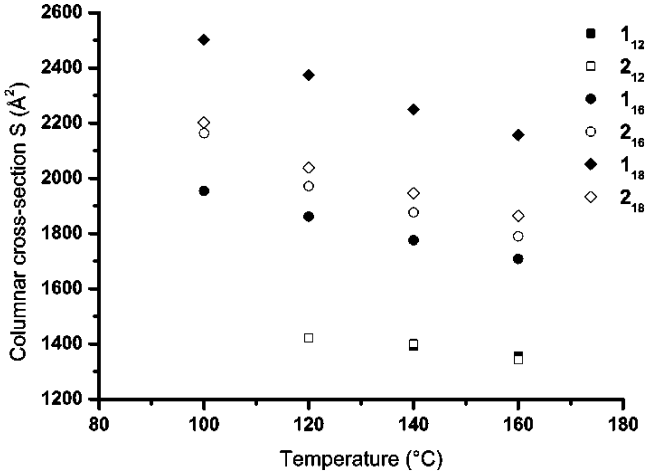

Figure 5. Variation of the columnar cross sections (Colh phases) with temperature, chain length, and counterion.

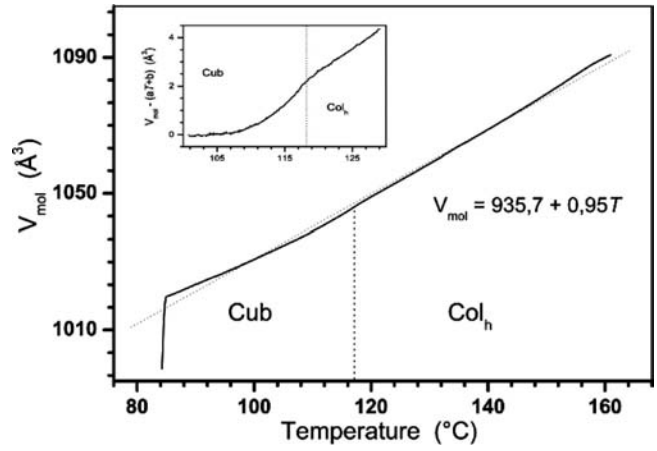

Figure 6. Molecular volume variation of $\mathbf{2_{12}}$ as function of temperature, determined by dilatometry.

to decrease with *T* in agreement with the increasing chain mobility and disorder. It can be observed that this decrease is strongly dependent on both the chain length and the counteranion. For instance, the slope increases very steeply as the chain length is augmented from 12 to 18 methylene units per chain, which suggests strong chain coiling and/or interdigitation for the longer chains' homologues. Moreover, while the increase in the cross section is quite regular for the chloride derivatives, we observe a settling as far as the bromides are concerned. This point will be discussed in the following.

2.3. Dilatometric Studies. Prior to the analysis of the molecular packing of the various compounds in their mesophases, the molecular volume (V_{mol}) of one salt, $\mathbf{2_{12}}$, was measured experimentally by dilatometry and its variation followed as a function of temperature. The experiment was carried out with approximately 1 g of compound, between room temperature and 160 °C, including the Cr-to-Cub and the Cub-to-Colh phase transformations (Figure 6). The molecular volume was found to augment with temperature in the stability range of each one of the phases observed. Upon cooling, the volume decreases quite reversibly in the whole range explored, and the cubic phase supercools, as usual, slightly below the melting temperature.

At ~80−81 °C in agreement with the results from optical microscopy and differential scanning calorimetry, the crystal-to-cubic phase transition was detected by an abrupt jump in the molecular volume, corresponding to the melting of the aliphatic chains. Then, above this transition, its temperature variation increases quasi-linearly despite the change from one mesophase to another (Cub-to-Colh), in common with other liquid crystals.[11] In detail, a slight change in the slope could be detected at the cubic-to-columnar phase transformation (at ca. 118 °C; see Figure 6), although this change remains meaningless, and in the following, only the linear variation over the entire temperature domain will be considered. The slope is in fairly good agreement with the volume variation in the methylene groups in liquid alkanes,[12] an indication that the aromatic component of the volume (V_{ar}) is almost unchanged with temperature in the mesophase (and will be considered thereafter as a fixed value over the mesomorphic temperature range) and that the molecular volume is dominated by that of the aliphatic chains. Therefore, the molecular volume V_{mol} can be written as a sum of elementary volumes associated with the different segments of the molecule according to $V_{mol}(T) = V_{ar} + V_{ch}(T)$, where V_{ar} is the volume of the rigid part, and $V_{ch}(T) = 2nV_{CH2}(T) = 2n(26.5616 + 0.02023T)$. Note that the contribution of the counterion to the molecular volume is negligible within the same series but also between series **1** and **2**, with a difference of less than 10 Å^3.

From the slope of the molecular variation of $\mathbf{2_{12}}$ as a function of temperature, with a linear fit approximation, the volume is found to be equal to $935.7 + 0.95T$, with *T* in degree Celsius. Thus, the volume of $\mathbf{2}_i$ or $\mathbf{1}_i$ can be written as $V_{mol}(\mathbf{2}_i/\mathbf{1}_i) = 935.7 + 0.95T + 2 \times (i - 12) \times (26.5616 + 0.02023T)$.

2.4. Supramolecular Organization in the Mesophases. 2.4.1. Smectic Phase. In smectic systems, it is practical to consider the molecular cross-sectional area, A_M. This parameter

(11) Mathevet, F.; Masson, P.; Nicoud, J.-F.; Skoulios, A. *Chem.—Eur. J.* **2002**, *8*, 2248.
(12) Doolittle, A. K. *J. Appl. Phys.* **1951**, *22*, 1471.

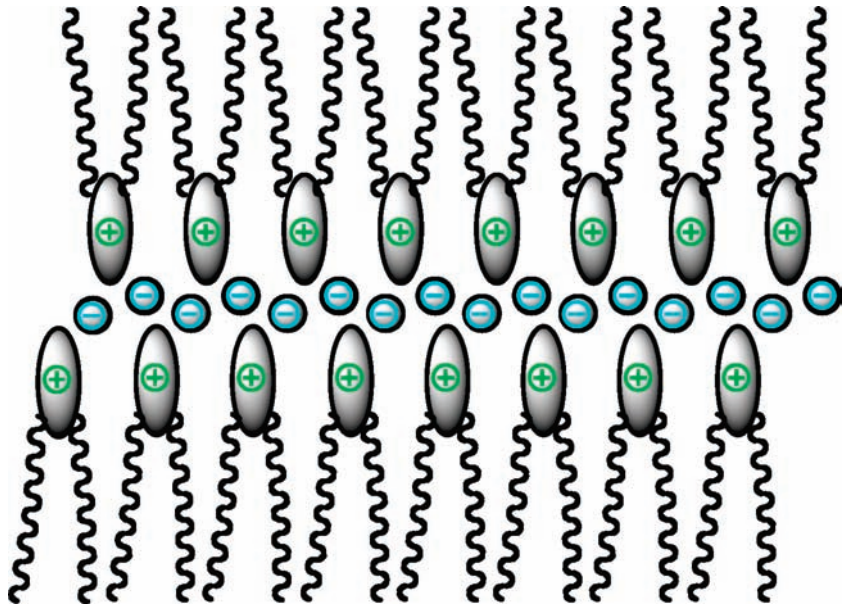

Figure 7. Schematic drawing of the possible arrangement of the imidazolium species and anions in an ionic double layer.

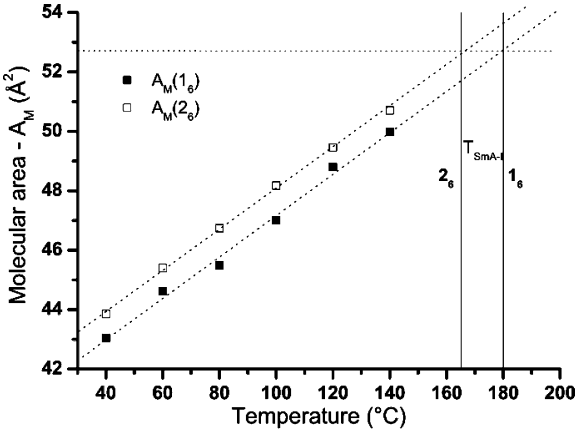

Figure 8. Molecular area variation in the smectic phase as a function of temperature and counterion ($\mathbf{1}_6$, $\mathbf{2}_6$).

permits evaluation of the lateral packing of the molecules within the smectic layers and, moreover, discrimination between mono- and bilayer smectic arrangements. Considering a cylindrical conformation for the elemental molecular assembly(ies), A_M is obtained by the ratio NV_{mol}/d, in which d is the layer periodicity measured by XRD, V_{mol} the molecular volume measured by dilatometry, and N the number of molecules ($N = 1$ or 2). Thus, after calculation, molecular areas were found to be compatible with a bilayer structure ($N = 2$), with two molecules coupled head-to-head through their ionic headgroups, and with the chains homogeneously distributed on either side of the ionic polar plane formed by the polar heads and the counterions (Figure 7). The area of derivative **2** is slightly larger than that of **1**, in good agreement with the slightly larger radius of the bromide with respect to the chloride ion. As the temperature is raised, the molecular area increases linearly (identical behavior for both compounds, same slope, Figure 8) concomitantly with the increasing disordering of the molten chains, until chain fluctuations become too strong and disorganize the layers' arrangements completely. An interesting geometrical relationship has been deduced between both compounds $\mathbf{1}_6$ and $\mathbf{2}_6$. Indeed, they both are clear when their molecular areas reach the same value close to 52.5 Å^2 (estimated by the linear fits as a function of temperature of the A_M temperature variations), at $T = 180$ and $T = 165$ °C, respectively (Figure 8), indicative that the process of layer destruction is the same for both compounds and is solely governed by the molecular cross-sectional area.

2.4.2. Columnar Phase. Due to the curvature of the aliphatic−ionic interface intervening at a longer chain length ($n \geq 12$), i.e., when the contribution of the aliphatic volume fraction is becoming the dominant factor, a finite number of molecules self-aggregate together in the head-to-head fashion (with the polar parts in the columns interior or spine) to generate the columns (or discs).[8b] The lateral dimension of the columns is significantly larger than twice the length of the molecules as estimated from molecular modeling (for example, $\mathbf{1}_{12}$ corresponds to 24.5 Å). These measurements strongly suggest that the molecules therefore are not stacked on top of each other in single rows but densely aggregated around the columnar axis.

From a geometrical point of view, the columnar structures are characterized mainly by two parameters: the columnar cross section (S) and the stacking periodicity along the columnar axis (h).[13] Knowledge of these two structural parameters permits interpretation of the molecular packing inside the columns.[14] S, h, and V_{mol} are linked analytically through the relation given by the equation $hS = NV_{mol}$, in which N is the number of molecules (or molecular equivalents) within a columnar stratum of thickness h and section S. It was found, for h fixed to 4.5 Å,[14] that N varies significantly as the function of the molecular structure (counterion and chain length) and with temperature (Figure 9). In all cases, the number of molecular equivalents per columnar stratum 4.5 Å thick decreasees with temperature, in concordance with the reduction of the columnar cross section. This result can be interpreted as the shrinkage and stretching of the columnar cores with increasing temperature with columnar undulations becoming less and less important. This effect is also

(13) Guillon, D. *Struct. Bonding (Berlin)* **1999**, *95*, 41.
(14) (a) Morale, F.; Date, R. W.; Guillon, D.; Bruce, D. W.; Finn, R. L.; Wilson, C.; Blake, A. J.; Schröder, M.; Donnio, B. *Chem.—Eur. J.* **2003**, *9*, 2484. (b) Donnio, B.; Heinrich, B.; Allouchi, H.; Kain, J.; Diele, S.; Guillon, D.; Bruce, D. W. *J. Am. Chem. Soc.* **2004**, *126*, 15258.

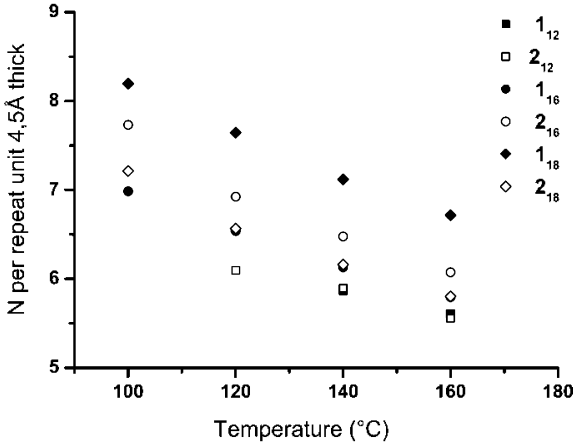

Figure 9. Variation of the number of molecular equivalents, *N*, as a function of temperature, chain length ($n = 12, 16, 18$) and couterion (**1** vs **2**).

attenuated with the length of the chains: the undulations are less and less perceptible as the chains increase, and even essentially absent at long chain length (for $n \geq 16$). As expected, the number of molecular equivalents per elementary columnar slice increases with increasing *n*, but this increase is strongly counterion dependent (Figure 9).

To further understand the self-organization inside the column, we have conducted molecular dynamic (MD) simulations in which a column model was built from the experimental X-ray data. In a first step the cation moiety of $\mathbf{2_{12}}$ was optimized with the AM1 semiempirical method (MOPAC 2007) to obtain reliable atomic electronic densities for the MD calculations. Then a hexagonal cell incorporating 12 molecules of $\mathbf{2_{12}}$ was built with *a* and *b* parameters set according to the X-ray lattice parameters and with a thickness calculated ($h \approx 9$ Å) so that the average density of the material is the same as that measured experimentally by dilatometry. After a few optimization steps, the cell was equilibrated with an isothermal 200 ps MD simulation in periodic boundary conditions. The resulting molecular arrangement showed a columnar backbone made from the bromide and polar part of the imidazolium moiety surrounded by molten alkyl chains, and the columnar cross section is fully filled (Figure 10). The columnar cross section does not

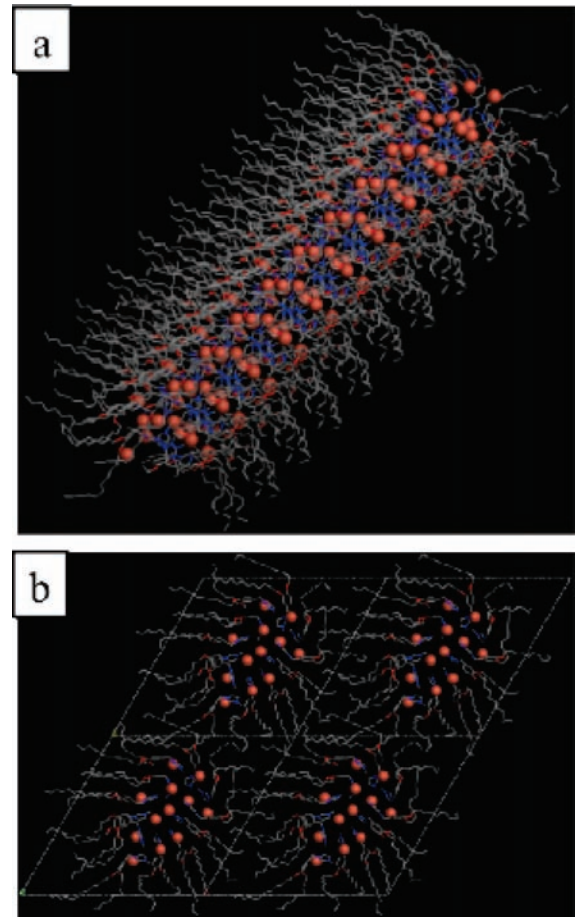

Figure 10. Snapshots showing (a) the molecular self-assembly of $\mathbf{2_{12}}$ into columns and (b) their packing in the hexagonal 2D network (polar central imidazolium with the nitrogen atoms in blue sheating with alkyloxy chains (oxygen atoms in red) and bromide counterion shown in pale red).

appear circular but is averaged along the columnar axes and from one column to another, giving rise to the appropriate 6-fold symmetry of the columnar phase.

2.4.3. Cubic Phase. While commonly induced in various binary lyotropic systems,[15] and being well described mathematically by films of constant thickness separating polar and nonpolar regions (the so-called infinite periodic minimal surfaces concept), the cubic mesophase with the $Ia\bar{3}d$ space group is rarely observed in thermotropic systems.[16] Moreover, its supramolecular organization is not yet completely understood, particularly on space filling geometrical grounds: indeed, the available volume must be completely filled by the mesogens, because it is not compensated by another constituent, such as water, as in the counterpart lyotropic phase. The structure of the thermotropic bicontinuous $Ia\bar{3}d$ cubic phase can be understood by the double-network structural model and consists of two intertwined, unconnected 3D networks of 24 short column segments, coplanarly linked 3×3 at each node of the network, and separated by the Gyroïd infinite periodic minimal surface. In this case, the most plausible hypothesis is to consider that the aromatic parts form two separate continuous interwoven networks of channels immersed in the aliphatic matrix, therefore adopting an inverse type structure (Figure 11).[10,15] From dilatometry, ~730 molecules are needed to completely fill the available volume of the cubic phase, i.e., 365 molecules per individual network. Moreover from dilatometry, approximately

(15) (a) Fontell, K. *Adv. Coll. Interface* **1992**, *41*, 127. (b) Seddon, J. M.; templer, R. H. *Phil. Trans. R. Soc. Lond. A* **1993**, *344*, 377.
(16) (a) Etherington, G.; Leadbetter, A. J.; Wang, X. J.; Gray, G. W.; Tajbakhsh, A. *Liq. Cryst.* **1986**, *1*, 209. (b) Kutsumizu, S.; Yamada, M.; Yano, S. *Liq. Cryst.* **1994**, *3*, 155. (c) Fischer, S.; Fischer, H.; Diele, S.; Pelzl, G.; Jankowski, K.; Schmidt, R. R.; Vill, V. *Liq. Cryst.* **1994**, *17*, 855. (d) Bruce, D. W.; Donnio, B.; Hudson, S. A.; Levelut, A. M.; Megtert, S.; Petermann, D.; Véber, M. *J. Phys. II (France)* **1995**, *5*, 289. (e) Donnio, B.; Heinrich, B.; Gulik-Krzywicki, T.; Delacroix, H.; Guillon, D.; Bruce, D. W. *Chem. Mater.* **1997**, *9*, 2951. (f) Tsiourvas, D.; Kardassi, D.; Paleos, C. M.; Gehant, S.; Skoulios, A. *Liq. Cryst.* **1997**, *23*, 269. (g) Paleos, C. M.; Kardassi, D.; Tsiourvas, D.; Skoulios, A. *Liq. Cryst.* **1998**, *25*, 267. (h) Göring, P.; Diele, S.; Fischer, S.; Wiegeleben, A.; Pelzl, G. *Liq. Cryst.* **1998**, *25*, 467. (i) Tsiourvas, D.; Paleos, C. M.; Skoulios, A. *Macromolecules* **1999**, *32*, 8059. (j) Kutsumizu, S.; Morita, K.; Ichikawa, T.; Nojima, S.; Yamaguchi, T. *Liq. Cryst.* **2002**, *29*, 1447. (k) Tsiourvas, D.; Stathopoulou, K.; Sideratou, Z.; Paleos, C. M. *Macromolecules* **2002**, *35*, 1746. (l) Neve, F.; Impéror-Clerc, M. *Liq. Cryst.* **2004**, *31*, 907. (m) Massiot, P.; Impéror-Clerc, M.; Veber, M.; Deschenaux, R. *Chem. Mater.* **2005**, *17*, 1946. (n) Kutsumizu, S.; Saito, K.; Nojima, S.; Sorai, M.; Galyametdinov, Y. G.; Galyametdinova, I.; Eidenschink, R.; Haase, W. *Liq. Cryst.* **2006**, *33*, 75. (o) Martin, J. D.; Keary, C. L.; Thornton, T. A.; Novotnak, M. P.; Knuston, J. W.; Folmer, J. C. W. *Nat. Mater.* **2006**, *5*, 271. (p) Kutsumizu, S.; Mori, H.; Fukatami, M.; Naito, S.; Sakajiri, K.; Saito, K. *Chem. Mater.* **2008**, *20*, 3675.

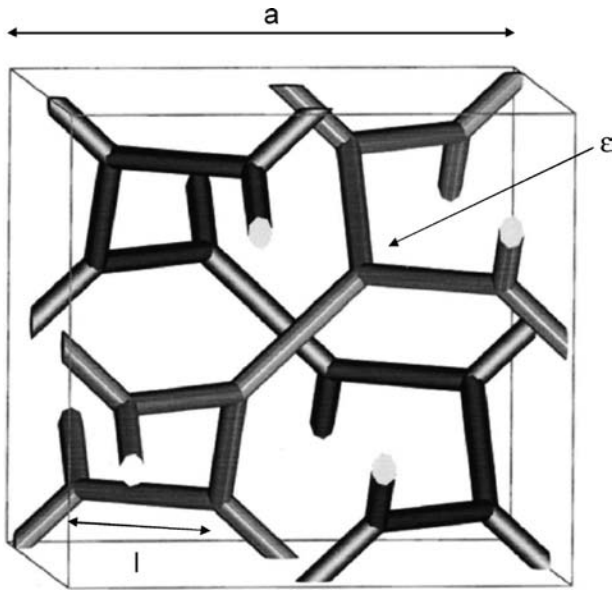

Figure 11. Schematic representation of the rod model associated to the $Ia\bar{3}d$ cubic symmetry: two interwoven unconnected networks linked 3×3 in a coplanar fashion (24 columns per unit cell). In the model, the rods are filled with the polar aromatic parts whereas the void is filled by the molten aliphatic chains (see text).

two-thirds of the cubic lattice is filled by molten aliphatic chains, whereas the networks correspond to the remaining third (the polar part).

A detailed description of the cubic phase structure is complicated because of the estimation of the volume (and shape) at the junctions of three different minicylinders. Indeed, the column segments are not perfectly joined end-to-end at these connections but separated by a short gap which depends on the diameter of the column segment, ϕ: therefore their length is smaller than in the case of columns joined without discontinuity ($\phi = 0$, i.e., mathematical lines). The distance between two ternary junctions forming the continuous network frame (elemental rod length), l_0, is directly related to the cubic lattice parameter $l_0 = a/\sqrt{8}$ ($\phi = 0$). However, when $\phi \neq 0$, this distance is reduced to $l_\phi = a/\sqrt{8} - \epsilon(\phi)$. Neither the evaluation of ϵ nor therefore the repartitioning of molecules within the cubic structure is straightforward. At these crystallographic positions, the number of molecules increases necessarily with respect to the monotonous distribution in the cylinders. In the present case, one can assume that the overall column integrity is kept during the Colh-to-Cub phase transformation (identical cross sections, $S_{Cub} = S_{Colh} = S$, where S_{cub} corresponds to the cross-columnar section of the minicolumn within the cubic phase), a reasonable hypothesis due to great molecular flexibility, and that, as the temperature is reduced, the columns formed by the piled polar aromatic cores in the Colh phase evolve into the rod networks, which are surrounded by the molten aliphatic chain continuum. This transformation may occur through regular column undulations and interconnections, which increase substantially with reducing temperature, to permit the formation of the two interlaced networks, similarly to the supramolecular model described earlier for the bistilbazole silver complexes.[16e]

2.5. Transfection Activities. Delivery of siRNA into cells is one of the major concerns for therapeutic applications of siRNA. Three stages are required for efficient siRNA delivery: (1) protection of nucleic acid, (2) its penetration into cells, and (3) its transfer inside the cytosol. Based on their structure, our molecules can have the capacity to achieve the three steps. The cationic part is able to bind the siRNA, whereas the liphophilic part enables the molecule to cross the lipids bilayers of cell membrane and go into cells. Compounds $\mathbf{2_{12}}$, $\mathbf{1_{12}}$, and $\mathbf{1_{18}}$ were evaluated for their ability to form a complex with synthetic siRNA using a gel retardation assay. Each compound was formulated at 1 mM with and without 2 mM of 1,2-dioleoyl-*sn*-glycero-3-phosphoethanolamine (DOPE) in water. A colipid was added to the cationic liposomal formulation not only to increase lipoplex fusogenicity but also to decrease their toxicity. DOPE was chosen as it can form the H_{11} phase structure known to induce supramolecular arrangement leading to the fusion of a lipid bilayer at a temperature greater than 5−10 °C. Its incorporation is also supposed to destabilize the endosomal membrane.[17] Constant amounts of siRNAs were mixed with increasing amounts of imidazolium-based formulations and loaded on agarose gel.

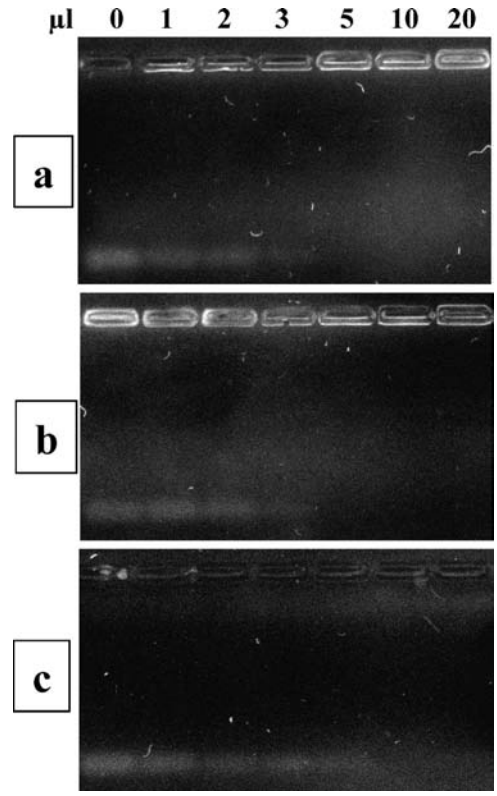

Figure 12. Electrophoresis on 1.2% agarose gel of complexes formed between siRNAs and $\mathbf{2_{12}}$ (a), $\mathbf{1_{12}}$ (b), $\mathbf{1_{18}}$ (c) compounds formulated with DOPE. 700 ng of siRNAs were complexed with increasing amount of formulated compound (1, 2, 3, 5, 10, and 20 μL, *i.e.*, 1, 2, 3, 50, 10, and 20 nmol of imidazolium).

These experiments (Figure 12) show the naked siRNA and the complexes, retained in the well, formed between the siRNAs, and $\mathbf{2_{12}}$-, $\mathbf{1_{12}}$-, and $\mathbf{1_{18}}$-based formulations. The results showed that siRNA binding to the compound tested is not affected by the counterion (Cl^- or Br^-), as the same volume of formulated $\mathbf{2_{12}}$, $\mathbf{1_{12}}$ is necessary to complex all the siRNAs. However, the length of the alkyl chain influenced the siRNA binding efficacy, as a higher amount of $\mathbf{1_{18}}$ is required to complex all the siRNAs. These data show the ability of our compounds to interact with siRNA and form complexes, the first property required for

(17) (a) Gruner, S. M.; Tate, M. W.; Kirk, G. L.; So, P. T.; Turner, D. C.; Keane, D. T.; et al. *Biochemistry* **1988**, *27*, 2853–2866. (b) Farhood, H.; Serbina, N.; Huang, L. *Biochim. Biophys. Acta* **1995**, *1235*, 289–295.

Table 2. Particle Size and Zeta Potential of siRNA (700 ng) Complexed with 4 μL of Formulated $\mathbf{1_{12}}$ and $\mathbf{1_{18}}$

formulation	size (nm)[a]	zeta potential (mV)
$\mathbf{1_{12}}$/DOPE/siRNA	68.7 ± 25.7	+61.1
$\mathbf{1_{18}}$/DOPE/siRNA	593 ± 25.7[b]	−0.28

[a] Each value represents the mean ± SD of 15 measurements. [b] Polydisperse particle sizes have been observed.

efficient siRNA delivery. Then, to bind to the cell surface and enter into cells, positively charged complexes are required. The physical properties such as surface charge and size of the particles were determined using Dynamic Light Scattering (DLS) measurements. These parameters influence cellular interactions and nanoparticle distribution. The size (mean around 70 nm) and zeta potential (highly positive) (Table 2) of the particles (complexes) formed between siRNA and the compound $\mathbf{1_{12}}$ are compatible with the first step based on the sticking of positively charged nanoparticles onto the plasma membrane, followed by endocytosis.

The neutral zeta potential of the particles formed with the $\mathbf{1_{18}}$-based formulation confirms its low ability to complex siRNAs and consequently is a sign of a probably low capacity to deliver synthetic genetic material into cells. Moreover, the size of the complex formed with compound $\mathbf{1_{18}}$ (*ca.* 600 nm) which is not suitable for cellular uptake indicated an aggregation tendency, suggesting a colloidal instability behavior not favorable for transfection. Then, the ability of each formulation to deliver siRNA into cells, in the presence of serum, was determined using fluorescently labeled siRNAs. 50 nM siRNAs labeled with Rhodamine and complexed with a constant amount of each formulation (*i.e.*, $\mathbf{2_{12}}$, $\mathbf{1_{12}}$, and $\mathbf{1_{18}}$) were delivered into a human lung carcinoma cell line stably expressing the luciferase (A459Luc cells). The fluorescence was observed 4 and 24 h after transfection. As shown in Figure 13, siRNAs delivered with compounds $\mathbf{2_{12}}$ and $\mathbf{1_{12}}$ are visible, associated to the cells 4 h after transfection. Fluorescence into the cells is more uniform 24 h after transfection with decreasing intensity, demonstrating intracellular release of the siRNAs from the endosomes into the cytoplasm (data not shown). With compound $\mathbf{1_{18}}$ complex aggregates were seen outside and not associated to the cells. Moreover, the number of cells transfected with the siRNAs is less important.

The presence of aggregates outside the cells confirms the size value obtained by DLS (Table 2). We show that compounds $\mathbf{2_{12}}$ and $\mathbf{1_{18}}$ have the ability to (1) bind to the cell and (2) transfer siRNA into the cytosol. However, functionality of the delivered siRNA has to be demonstrated. Then, A549Luc cells, stably expressing the luciferase gene, were used as a model system. Luciferase specific and mismatch siRNAs (10 and 1 nM) were delivered after complexation with a constant amount of formulated $\mathbf{2_{12}}$-, $\mathbf{1_{12}}$-, and $\mathbf{1_{18}}$-based formulations. The luciferase expression was determined 48 h after transfection. As a positive control for transfection, Lipofectamine2000 was used in this experiment. Figure 14 shows that the luciferase level, expressed relative to the level obtained with the mismatch siRNAs, was reduced by 70−80% when siRNAs (10 nM) were delivered using $\mathbf{2_{12}}$ and $\mathbf{1_{12}}$ formulated with DOPE. No significant luciferase inhibition (<5%) was observed by using the mismatch siRNA (data not shown).

These two formulations ($\mathbf{2_{12}}$ and $\mathbf{1_{12}}$) are still significantly efficient, even at a low siRNA concentration of 1 nM. To confirm the necessity of a cohelper lipid, compound $\mathbf{1_{12}}$ was also formulated with different amounts of DOPE (from 0 mM to 4 mM). At 10 nM, the highest inhibition was observed with the formulation 1:2 (1 mM imidazolium:2 mM DOPE). A strong toxicity was observed with the ratio 1:1 (data not shown). These data confirm that the use of a colipid is necessary to increase transfection efficiency. It is also shown that, in our case, the best ratio between the cationic liposomal formulation and the colipid is 1:2. As expected because of its low siRNA binding efficacy, the inhibition obtained with the $\mathbf{1_{18}}$-based formulation was lower (<30% at 10 nM of siRNA) confirming that the length of the alkyl chain is important for the delivery of active siRNA.

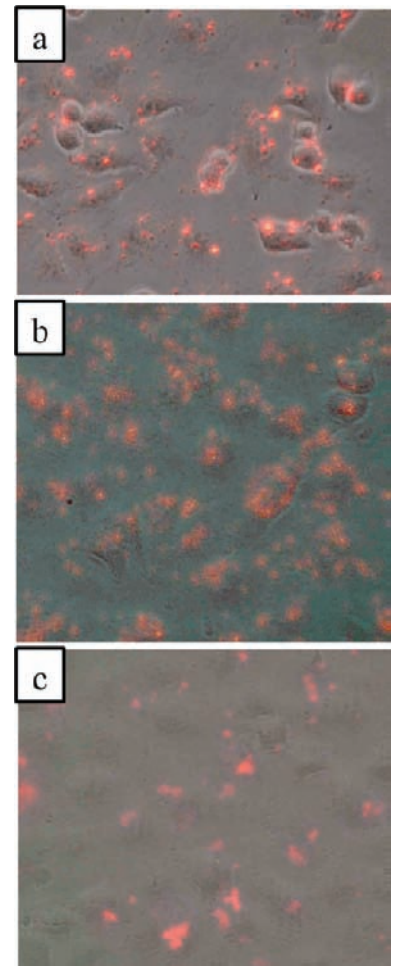

Figure 13. A549Luc cells were transfected with 50 nM Rhodamine labeled siRNAs complexed with 6 μL of $\mathbf{2_{12}}$ (a), $\mathbf{1_{12}}$ (b), $\mathbf{1_{18}}$ (c) compounds formulated with DOPE. Fluorescence was observed 4 h after transfection using a microscope.

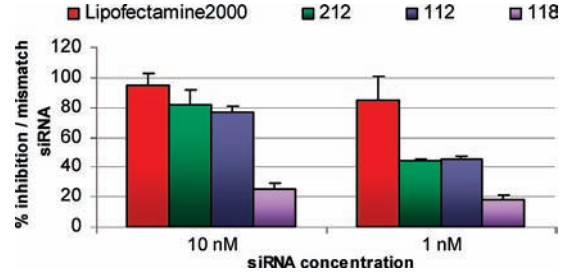

Figure 14. A549Luc cells, stably expressing the luciferase gene, were transfected with luciferase specific siRNA complexed with $\mathbf{1_{12}}$, $\mathbf{2_{12}}$, and $\mathbf{1_{18}}$ formulated with DOPE. As a positive control, Lipofectamine2000 was included in the experiment. Luciferase gene expression was measured 48 h after transfection.

Taken together, our results show that successful gene silencing can be achieved with imidazolium-based formulations (exemplified with $\mathbf{2}_{12}$ and $\mathbf{1}_{12}$ compounds) when formulated with a colipid DOPE, a well-known cohelper phospholipid for transfection. We showed also that the length of the alkyl chain of the imidazolium compound has to be optimized for an efficient binding of siRNA, as well as for efficient gene silencing in cells. As transfection is not restricted to siRNA binding and plasma membrane sticking, this suggest also that the imidazolium moiety exhibits the required properties to efficiently achieve the intracellular transfection steps leading to the final release of siRNA inside the cytoplasm.

3. Summary

In conclusion, we have prepared new dicatenar imidazolium compounds exhibiting a smectic A mesophase for short alkyl chains and a columnar hexagonal phase constituted of aggregates for long tails. We have also characterized a rare example of an $Ia\bar{3}d$ bicontinuous cubic phase with this imidazolium head. These salts not only show thermotropic properties but also are promising amphiphilic molecules for siRNA delivery when formulated with colipids. It is also noteworthy that only the compounds bearing dodecyl tails ($\mathbf{1}_{12}$ and $\mathbf{2}_{12}$) exhibit both cubic and columnar phases as well as show greater ability to encapsulate siRNA and a higher transfection yield. We are now attempting to investigate the lyotropic behavior of these compounds.

Acknowledgment. We are especially grateful to Dr. J. Harrowfield for critical evaluation of the manuscript. This work was supported by the CNRS and University of Strasbourg.

Supporting Information Available: Experimental procedures, products characterization (spectroscopic and analytical data), biological experimental section, including the synthesis of siRNA and X-ray experimental data of the mesophases. This material is available free of charge via the Internet at http://pubs.acs.org.

JA903028F